Structure and Properties of Poly-bis(μ-monophenylphosphinato)bis(formamide) Chain Polymers of Cadmium(II), Manganese(II) and Cobalt(II). Antiferromagnetic Exchange in the Manganese and Cobalt Compounds

PETER BETZ, AVI BINO*

Department of Inorganic and Analytical Chemistry, The Hebrew University of Jerusalem, 91904 Jerusalem (Israel)

JING-LONG DU, LINDA S.-M. LO and ROBERT C. THOMPSON*

Department of Chemistry, University of British Columbia, 2036 Main Mall, Vancouver, B.C., V6T 1Y6 (Canada)

(Received September 4, 1989)

Abstract

The compounds $M(HCONH_2)_2[H(C_6H_5)PO_2]_2$ where M = Co (**1**), Cd (**2**) and Mn (**3**) were synthesized and characterized using single crystal X-ray diffraction, differential scanning calorimetry, infrared spectroscopy and magnetic susceptibility (2 to 80 K) studies. The three compounds are isomorphous, their structures consisting of polymeric chains, propagating along the crystallographic *b* axis, in which two phosphinate ligands form double bridges between adjacent metal atoms. Two formamide molecules are coordinated via oxygen to each metal atom, completing an octahedral geometry. Compounds **1** and **3** are antiferromagnetic exhibiting maxima in their χ_m versus T plots at 6.3 and 5.8 K respectively. The magnetic data for the Mn(II) compound have been successfully analyzed according to the Weng and Wagner–Friedberg Heisenberg models for linear chains with exchange coupling constants of -0.47 and -0.51 cm^{-1} respectively. Magnetic susceptibilities for the Co(II) compound have been compared to values calculated using five different theoretical models. Suitable fits over the range 2 to 80 K were not obtained; however, the data below 30 K agree reasonably well with both Ising and Heisenberg models employing an effective spin $S' = 1/2$.

Introduction

A large number of metal phosphinate compounds have been reported, most of which are polymeric, typically exhibiting a structure in which chains of metal atoms are linked by double phosphinate bridges [1]. Where a paramagnetic metal is involved, magnetic susceptibility studies are of particular interest because of the potential for magnetic exchange propagated via the bridging phosphinate groups. Some correlation between the nature and magnitude of exchange with structure has been found as, for example, in the case of the dialkylphosphinates of copper(II) where both ferromagnetic and antiferromagnetic behaviour have been observed. These compounds have compressed tetrahedral stereochemistries (D_{2d} local symmetry about copper) and the nature of the exchange has been correlated with the degree of compression of the CuO_4 chromophore [2]. The local environment about copper in the polymeric diphenylphosphinate derivative on the other hand, is square planar [3] and ferromagnetic exchange was observed for this material [4]. Compared to copper little has been reported on magneto-structural correlations in phosphinates of manganese(II) and cobalt(II). The structure of $Mn(H_2O)_2[(CH_3)_2PO_2]_2$ involves square planar MnO_4 units formed by bridging phosphinate groups with water molecules bonded axially and completing octahedral coordination about manganese. Studies to 4.2 K gave no conclusive evidence for magnetic exchange in this compound; upon dehydration, however, it shows relatively strong antiferromagnetic exchange [5]. Some synthetic, spectroscopic, and limited magnetic studies have been reported on a few other manganese(II) and cobalt(II) phosphinates [6].

We describe here the synthesis and structure determination of polymeric formamide adducts of some metal monophenylphosphinates with the composition $M(HCONH_2)_2[H(C_6H_5)PO_2]_2$, where M = Co (**1**), Cd (**2**) and Mn (**3**). Some spectroscopic and thermal analysis data are reported as are the magnetic susceptibilities (~80 to 2 K) of **1** and **3**.

Experimental

Synthesis

Crystals of **1**, **2** and **3** suitable for X-ray structural studies were obtained by dissolving the appropriate

*Authors to whom correspondence should be addressed.

0020-1693/90/$3.50

metal salt ($CoCl_2 \cdot 6H_2O$, 120 mg; $Cd(NO_3)_2 \cdot 4H_2O$, 150 mg; $Mn(ClO_4)_2 \cdot 6H_2O$, 130 mg) and 140 mg of $H(C_6H_5)PO_2H$ in a mixture of 2 ml of formamide and 20 ml of acetone and allowing the solution to concentrate by evaporation in an open beaker. Larger quantities of **1** and **3**, required for the magnetic studies, were obtained as follows. $H(C_6H_5)PO_2H$ (1.71 g) was added to a solution of $CoCl_2 \cdot 6H_2O$ (1.11 g) in acetone (150 ml) and formamide (16.6 ml). The solution was concentrated to approximately 10% of its original volume by evaporation in air over a period of about one week. The light purple powder (with some crystals) was washed with acetone and air dried. *Anal.* Calc. for $CoC_{14}H_{18}O_6N_2P_2$: C, 39.00; H, 4.21; N, 6.50. Found: C, 38.80; H, 4.35; N, 6.65%. $H(C_6H_5)PO_2H$ (0.926 g) was added to a solution of $Mn(ClO_4)_2 \cdot 6H_2O$ (0.832 g) in acetone (1.35 ml) and formamide (13.5 ml). The solution was stirred in an open beaker for about 20 h and the precipitate which formed was washed with acetone and air dried overnight. *Anal.* Calc. for $MnC_{14}H_{18}O_6N_2P_2$: C, 39.36; H, 4.25; N, 6.56. Found: C, 39.20; H, 4.42; N, 6.78.

Elemental analyses were performed by P. Borda, Microanalytical Laboratory, Department of Chemistry, University of British Columbia.

Infrared Spectra

Infrared spectra over the range of 4000 to 200 cm^{-1} were obtained using a Perkin-Elmer 598 infrared spectrometer. The samples were mulled in Nujol and pressed into a thin film between KRS-5 plates (Harshaw Chemical Co.). Frequencies reported are considered accurate to ± 5 cm^{-1} for broad bands and ± 2 cm^{-1} for sharp bands.

Differential Scanning Calorimetry (DSC)

DSC studies were made using a Mettler DSC 20 cell and a Mettler TC10 TA processor.

Magnetic Susceptibilities

Magnetic susceptibilities from 80 to 2 K were measured using a PAR model 155 vibrating sample magnetometer as described previously [7]. Measurements were made at a field of 7501 G. The diamagnetic corrections used were: -14, -12, -22 and -78×10^{-6} cm^3 mol^{-1} for Mn^{2+}, Co^{2+}, $HCONH_2$ and $H(C_6H_5)PO_2^-$ (and $H(C_6H_5)PO_2H$) respectively.

X-ray Crystallography

Data were collected at 20 ± 2 °C on a Philips PW 1100 four-circle diffractometer. Mo Kα ($\lambda = 0.71069$ Å) radiation with a graphite crystal monochromator in the incident beam was used. The unit cell dimensions were obtained by a least-squares fit of 20 reflections in the range of $12° < \theta < 16°$. Data were measured by using ω–2θ motion. Crystallographic data and other pertinent information are given in Table 1. For each crystal Lorentz and polarization corrections were applied. The heavy atom positions in structure **1** were obtained by using the results of SHELX 86 direct method analysis. Compounds **1**, **2** and **3** are isomorphous, their structures were refined* in space group $P2_1/c$ to convergence by using anisotropic thermal parameters for all non-hydrogen atoms and isotropic ones for the hydrogen atoms in **1** and **2**. The positional parameters of all

*All crystallographic computing was done on a CYBER 855 computer at the Hebrew University of Jerusalem, using the SHELX 1977 structure determination package.

TABLE 1. Crystallographic data

Compound	**1**	**2**	**3**
Formula	$C_{14}H_{18}CoN_2O_6P_2$	$C_{14}H_{18}CdN_2O_6P_2$	$C_{14}H_{18}MnN_2O_6P_2$
Formula weight	431.18	484.65	427.19
Space group	$P2_1/c$	$P2_1/c$	$P2_1/c$
a (Å)	10.453(1)	10.490(2)	10.456(2)
b (Å)	5.539(1)	5.756(1)	5.650(1)
c (Å)	14.587(2)	14.792(2)	14.674(2)
β (°)	96.47(2)	96.45(2)	96.21(3)
V (Å^3)	839(1)	887(1)	862(1)
Z	2	2	2
ρ_{calc} (g cm^{-3})	1.706	1.813	1.646
μ (cm^{-1})	11.68	13.21	9.11
Range of 2θ (°)	4–55	4–55	4–55
No. unique data	1889	1980	1987
Data with $F_o^2 > 3\sigma(F_o^2)$	1457	1431	1360
R	0.050	0.036	0.047
R_w	0.053	0.040	0.049

hydrogen atoms in **1**, **2** and **3** and a common thermal parameter for all phenyl and formamide hydrogen atoms in structure **3** were included in the least-squares refinement cycles.

The discrepancy indices $R = \Sigma||F_o| - |F_c||/\Sigma|F_o|$ and $R_w = [\Sigma w(|F_o| - |F_c|)^2/\Sigma w|F_o|^2]^{1/2}$ are listed in Table 1.

Results and Discussion

Crystal Structure Analysis

Compounds **1**, **2** and **3** are isomorphous. Tables 2, 3 and 4 present their positional parameters, respectively, and Table 5 presents important bond distances and angles. Figure 1 shows the structure of **1** and

TABLE 2. Positional parameters and e.s.d.s for **1**[a]

Atom	*x*	*y*	*z*	Atom	*x*	*y*	*z*
Co	0.000	0.000	0.000	C(7)	0.1576(4)	0.0464(8)	−0.1703(3)
P	0.1585(1)	0.4935(2)	0.05239(7)	N	0.0748(5)	0.190(1)	−0.2166(3)
O(1)	0.0970(3)	0.2618(6)	0.0831(2)	H(1)	0.158(4)	0.478(9)	−0.041(3)
O(2)	0.0993(3)	0.7255(6)	0.0816(2)	H(2)	0.352(4)	0.159(9)	0.036(3)
O(3)	0.1540(3)	−0.0184(7)	−0.0888(2)	H(3)	0.584(5)	0.15(1)	0.080(4)
C(1)	0.3274(4)	0.4873(9)	0.0936(3)	H(4)	0.689(6)	0.50(1)	0.163(4)
C(2)	0.4009(5)	0.2895(9)	0.0705(3)	H(5)	0.563(6)	0.80(1)	0.204(4)
C(3)	0.5334(5)	0.290(1)	0.0957(4)	H(6)	0.341(5)	0.83(1)	0.162(3)
C(4)	0.5917(5)	0.479(1)	0.1451(4)	H(7)	0.226(5)	−0.00(1)	−0.209(3)
C(5)	0.5195(5)	0.673(1)	0.1702(4)	H(8)	0.088(5)	0.21(1)	−0.267(4)
C(6)	0.3873(4)	0.6782(9)	0.1429(3)	H(9)	0.012(5)	0.27(1)	−0.189(4)

[a]e.s.d.s in the least significant digits are shown in parentheses.

TABLE 3. Positional parameters and e.s.d.s for **2**[a]

Atom	*x*	*y*	*z*	Atom	*x*	*y*	*z*
Cd	0.000	0.000	0.000	C(7)	0.1612(5)	0.0484(8)	−0.1751(4)
P	0.1639(1)	0.4959(3)	0.05763(7)	N	0.0757(6)	0.187(1)	−0.2167(4)
O(1)	0.1026(4)	0.2751(7)	0.0880(3)	H(1)	0.155(4)	0.49(1)	−0.031(3)
O(2)	0.1068(4)	0.7202(7)	0.0883(3)	H(2)	0.362(4)	0.17(1)	0.046(4)
O(3)	0.1629(4)	−0.017(1)	−0.0950(3)	H(3)	0.583(5)	0.16(1)	0.081(4)
C(1)	0.3332(4)	0.485(1)	0.0946(3)	H(4)	0.687(6)	0.45(1)	0.165(4)
C(2)	0.4047(5)	0.297(1)	0.0729(4)	H(5)	0.560(6)	0.79(1)	0.201(5)
C(3)	0.5360(5)	0.291(1)	0.0979(4)	H(6)	0.347(5)	0.80(1)	0.157(4)
C(4)	0.5954(5)	0.473(2)	0.1469(4)	H(7)	0.225(6)	−0.03(1)	−0.214(4)
C(5)	0.5255(6)	0.660(1)	0.1696(5)	H(8)	0.092(5)	0.21(1)	−0.273(4)
C(6)	0.3938(5)	0.672(1)	0.1430(4)	H(9)	0.002(9)	0.23(2)	−0.183(6)

[a]e.s.d.s in the least significant digits are shown in parentheses.

TABLE 4. Positional parameters and e.s.d.s for **3**[a]

Atom	*x*	*y*	*z*	Atom	*x*	*y*	*z*
Mn	0.000	0.000	0.000	C(7)	0.1577(4)	0.0483(9)	−0.1734(3)
P	0.16134(9)	0.4959(2)	0.05448(7)	N	0.0763(5)	0.1933(9)	−0.2170(3)
O(1)	0.0996(3)	0.2687(6)	0.0836(2)	H(1)	0.157(4)	0.483(9)	−0.039(3)
O(2)	0.1027(3)	0.7235(6)	0.0845(2)	H(2)	0.372(5)	0.16(1)	0.038(4)
O(3)	0.1564(3)	−0.0166(7)	−0.0929(2)	H(3)	0.584(5)	0.16(1)	0.078(4)
C(1)	0.3306(4)	0.4902(3)	0.0939(3)	H(4)	0.684(5)	0.48(1)	0.162(3)
C(2)	0.4027(5)	0.2941(9)	0.0712(3)	H(5)	0.558(5)	0.80(1)	0.205(4)
C(3)	0.5346(5)	0.290(1)	0.0966(4)	H(6)	0.350(5)	0.81(1)	0.164(4)
C(4)	0.5934(4)	0.477(1)	0.1459(3)	H(7)	0.224(5)	−0.02(1)	−0.213(3)
C(5)	0.5223(5)	0.667(1)	0.1704(3)	H(8)	0.084(5)	0.23(1)	−0.269(4)
C(6)	0.3905(4)	0.6767(9)	0.1432(3)	H(9)	0.014(5)	0.26(1)	−0.175(4)

[a]e.s.d.s in the least significant digits are shown in parentheses.

numbering scheme in all three compounds. Figure 2 shows a stereoscopic view of a section of the polymeric chain in all three compounds.

TABLE 5. Bond distances (Å) and bond angles (°)

Structure	M = Co(1)	M = Cd(2)	M = Mn(3)
M--O(1)	2.079(3)	2.247(4)	2.149(3)
M--O(2)'	2.128(3)	2.286(4)	2.201(3)
M--O(3)	2.179(3)	2.333(4)	2.241(3)
O(1)–M–O(2)'	90.2(1)	90.4(2)	89.8(1)
–O(2)''	89.8(1)	89.6(2)	90.2(1)
–O(3)	92.0(1)	92.5(2)	92.1(1)
–O(3)'	88.0(1)	87.5(2)	87.9(1)
O(2)'–M–O(3)	92.7(1)	91.8(2)	91.8(1)
–O(3)'	87.3(1)	88.2(2)	88.2(1)

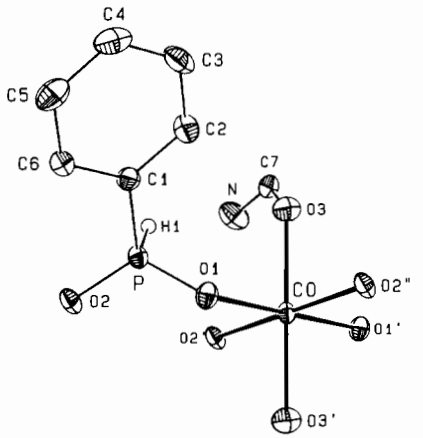

Fig. 1. View of $Co(HCONH_2)_2[H(C_6H_5)PO_2]_2$ showing the numbering scheme in 1, 2 and 3 and the coordination about the cobalt atom.

Structures 1, 2 and 3 consist of polymeric chains, propagating along the crystallographic *b* axis, in which two phosphinate ligands form double O–P–O bridges between adjacent metal atoms. The bridging phosphinates form square planar MO_4 units and six-coordination about the metal is achieved by axially O-bonded formamide ligands. The intrachain distance between metal atoms in 1, 2 and 3 are 5.539(1), 5.756(1) and 5.650(1) Å, respectively. Intramolecular hydrogen bonds between the NH_2 group of the coordinated formamide and an oxygen atom of a bridging phosphinate, exist in all structures with N....O(2) separation of about 2.9 Å. The second NH_2 hydrogen atom on each formamide ligand is involved in a hydrogen bond with a phosphinate oxygen of a neighboring chain with N....O(1) distance of about 2.9 Å.

Differential Scanning Calorimetry

$Co(HCONH_2)_2[H(C_6H_5)PO_2]_2$ (1) exhibits a sharp endothermic peak at 137 °C followed immediately by a broad endothermic event extending from about 140 to 170 °C (ΔH total for both events = 410 J g^{-1}; weight loss measurements confirm loss of two mol of $HCONH_2$). A third endothermic event occurs at 232 °C (ΔH = 92 J g^{-1}) due to melting (confirmed by visual observation in a melting point apparatus). Onset of exothermic decomposition occurs at about 265 °C. Both 2 and 3 show similar two-component endotherms corresponding to loss of the two formamide ligands. For 3 the events are at 140 and ~190 °C (ΔH = 256 J g^{-1} for both events) and for 2 they occur at 150 and ~180 °C (ΔH = 307 J g^{-1} for both events). Both 2 and 3 oxidatively decompose without melting with the process beginning at about 220 and 270 °C respectively.

In summary 1, 2 and 3 all undergo stepwise loss of formamide ligands in the 130 to 190 °C temperature range yielding the corresponding non-ligated metal

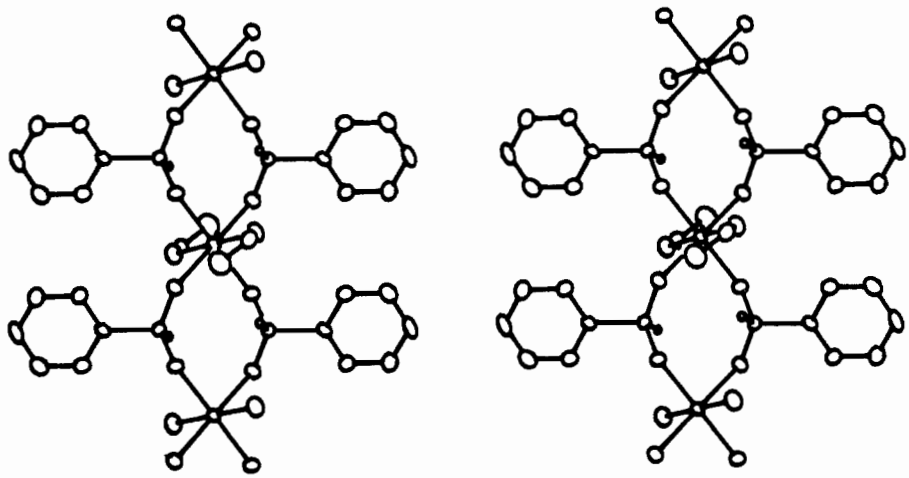

Fig. 2. Stereoview of a section of $M(HCONH_2)_2[H(C_6H_5)PO_2]_2$.

phosphinate derivative. Of these, only the cobalt compound melts without decomposition.

Infrared Spectra

The infrared spectra of **1**, **2** and **3** are virtually indistinguishable as would be expected for isostructural compounds. The compounds exhibit broad, medium intensity, structured absorptions centred around 3180 cm^{-1} (maxima at −3240 and 3120 cm^{-1}) due to NH_2 stretching and a strong broad band at 1670 cm^{-1} (shoulder at ~1690 cm^{-1}) due to CO stretching. This compares with corresponding bands at approximately 3310 and 1680 cm^{-1} in pure $HCONH_2$ and the greater shift in $\nu(NH_2)$ compared to the shift in $\nu(CO)$ shows that in spite of the fact that formamide is coordinated through oxygen a greater perturbation is caused by the hydrogen bonding involving the NH_2 groups. The PO_2 antisymmetric stretching vibrations appear as strong broad bands at 1130 cm^{-1} and the symmetric stretching modes are of medium intensity at 1040 (**1** and **2**) and 1046 (**3**) cm^{-1}. These band frequencies are comparable to those observed for $Cu[(C_6H_5)_2PO_2]_2$ [4] and the dialkylphosphinates of copper(II) [2] and are consistent with the relatively symmetrical phosphinate bridging in these compounds. Relatively sharp medium intensity bands ascribed to P–H stretching vibrations occur at 2402, 2390 and 2380 cm^{-1} for **1**, **2** and **3** respectively.

Magnetic Susceptibilities

Magnetic susceptibility and magnetic moment data for **1** and **3** are recorded in Table 6. The $^6A_1$ ground state of the Mn(II) compound, **3**, leads to a relatively clear interpretation of its magnetic properties. The χ_m versus T plot shows a maximum at 5.8 K (Fig. 3), behaviour typical for an antiferromagnetically coupled system. The intrachain metal–metal distance is too large to allow for direct exchange and a superexchange mechanism involving the bridging phosphinates is almost certainly involved here. The data were analyzed as described previously [5] using the scaling model of Wagner and Friedberg [8] and the interpolation scheme developed by Weng [9] employing the equations and coefficients given by Hiller *et al.* [10]. The best fit values for the exchange coupling constant J are −0.47 cm^{-1} for the Weng model ($F = 0.0402$) and −0.51 cm^{-1} for the Wagner and Friedberg model ($F = 0.0436$). In both fits the value of g was set at 2.00. The fitting function, F, is defined in ref. 5. It is interesting to compare these fits to those obtained previously for $Mn[(CH_3)_2PO_2]_2$ [5]. As in the previous study, the fit employing the Weng model is slightly better than that employing the other model, as judged by the relative magnitudes of F. However, again as before, the Weng model does not reproduce the position of the rounded maximum in the χ_m plot as well. The comparison between experiment and theory for the Wagner–Friedberg model is illustrated in Fig. 3.

TABLE 6. Magnetic data

$Mn(HCONH_2)_2[H(C_6H_5)PO_2]_2$			$Co(HCONH_2)_2[H(C_6H_5)PO_2]_2$		
T (K)	$10^3 \times \chi_m$ ($cm^3\ mol^{-1}$)	$\mu(\mu_B)$	T (K)	$10^3 \times \chi_m$ ($cm^3\ mol^{-1}$)	$\mu(\mu_B)$
2.21	159	1.68	2.30	78.2	1.20
2.50	200	2.00	2.88	83.1	1.38
3.37	202	2.33	3.08	85.8	1.45
4.12	209	2.62	3.55	93.0	1.62
4.38	211	2.72	4.22	94.9	1.79
4.93	212	2.89	4.93	99.5	1.98
5.61	214	3.10	5.84	103	2.19
5.84	214	3.16	6.30	103	2.28
6.72	213	3.39	6.37	103	2.29
7.55	210	3.56	8.04	103	2.57
7.67	209	3.58	11.1	96.1	2.92
8.00	207	3.64	15.3	85.5	3.23
9.56	199	3.90	16.2	83.2	3.28
10.6	193	4.04	21.2	72.6	3.51
11.2	188	4.11	26.3	64.3	3.68
13.6	174	4.35	31.1	58.1	3.80
14.6	167	4.42	40.2	49.7	4.00
16.1	159	4.52	47.6	44.8	4.13
17.5	152	4.62	54.1	41.3	4.23
21.3	135	4.80	60.0	38.6	4.30
24.0	125	4.90	65.3	36.7	4.38
26.0	118	4.95	69.4	35.2	4.42
28.5	111	5.03	74.2	33.7	4.47
30.4	106	5.08	77.5	32.7	4.50
35.9	93.3	5.17	81.2	31.6	4.53
40.1	84.9	5.22			
46.4	75.8	5.30			
53.1	67.5	5.36			
60.4	60.9	5.42			
70.1	53.7	5.49			
81.7	46.8	5.53			

There are important structural similarities between **3** and the previously studied compound, $Mn(H_2O)_2[(CH_3)_2PO_2]_2$ [5]. Both have infinite chains of Mn atoms connected by double phosphinate bridges with four oxygens from different phosphinates forming a square planar array around each Mn. Neutral ligands coordinated on either side of the plane complete an MnO_6 chromophore. Hydrogen atoms on the neutral ligands are involved in both intrachain and interchain hydrogen bonding to bridging phosphinate groups in both compounds. In spite of these similarities the magnetic properties of these two materials differ significantly. The formamide compound studied here is clearly antiferromagnetic whereas no significant antiferromagnetic exchange was detected in the aqua compound [5]. It is possible that the hydrogen-bonding interactions are having a significant damping effect on the magnetic exchange in both of these

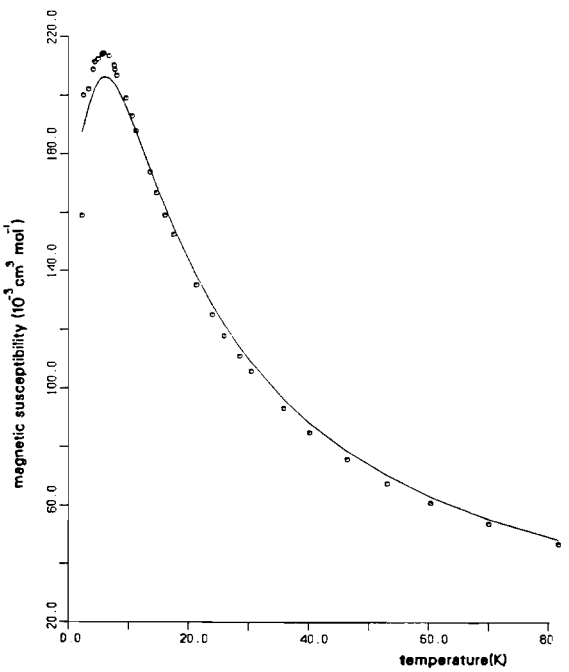

Fig. 3. Magnetic susceptibility vs. temperature plot for **3**. Line is the best fit to the Wagner–Friedberg model.

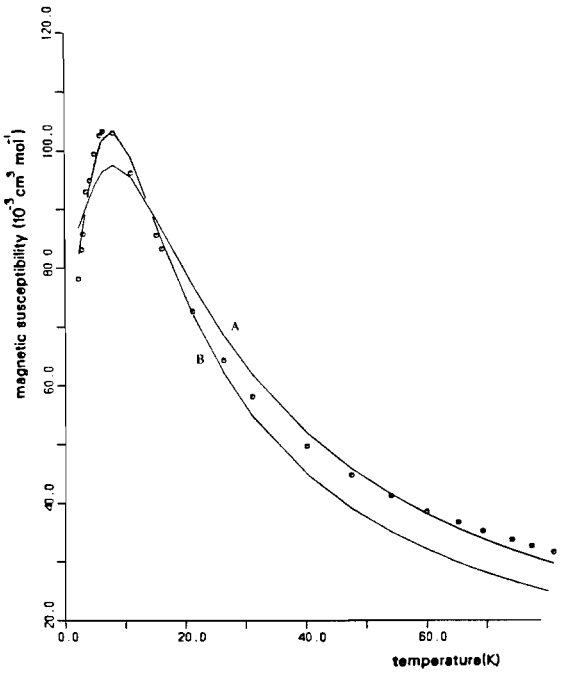

Fig. 4. Magnetic susceptibility versus temperature for **1**: A, line is best fit the Wagner–Friedberg $S = 3/2$ model; B, line is best fit to the Weng $S = 1/2$ model with data fitted over the 2–30 K range only.

compounds. The anhydrous forms of both $Mn[(CH_3)_2PO_2]_2$ and $Mn[H(C_6H_5)PO_2]_2$ are antiferromagnetic with maxima in χ_m versus T at 34 and 35 K and values of $J = -2.69$ and -2.78 cm^{-1} (Weng model) respectively [5, 11]. The effect of the aqua ligands in $Mn(H_2O)_2[(CH_3)_2PO_2]_2$ is to reduce this exchange effectively to zero ($|J| < 0.02$ cm^{-1} [5]) whereas the formamide ligands in $Mn(HCONH_2)_2$-$[H(C_6H_5)PO_2]_2$ reduce $|J|$ to 0.47 cm^{-1}. The hydrogen-bonding interactions in the aqua compound, particularly the interchain interactions, appear to be slightly stronger (O–H....O, interchain distance = 2.734(2) Å [5]) than those in the formamide compound (N–H....O, interchain distances = 2.9 Å) and this may account for the greater damping of exchange in the aqua complex.

The magnetic moment of $Co(HCONH_2)_2[H$-$(C_6H_5)PO_2]_2$ (**1**) decreases dramatically from 4.53 μ_B at 81 K to 1.2 μ_B at 2.30 K (Table 6) and the magnetic susceptibility exhibits a maximum at 6.3 K (Fig. 4). Although the magnetic moment of cobalt(II) ($^4T_{1g}$ ground state in O_h) in a distorted octahedral environment is expected to be temperature dependent [12], the magnitude of the temperature dependence of the moment, and more importantly the observation of a maximum in the χ_m versus T plot, is not consistent with magnetically dilute cobalt(II). The presence of antiferromagnetic coupling propagated via a superexchange mechanism involving the bridging phosphinate ligands (as observed in **3**) is clearly indicated.

The magnetic properties of an isolated Co(II) ion in a distorted octahedral environment are affected by factors such as electron delocalization, spin–orbit coupling, distortions from regular stereochemistry and the admixture of excited electronic states into the ground state by the crystal field [12]. The presence of antiferromagnetic coupling in **1** in addition to the above factors complicates the interpretation of the magnetic properties of this compound. The problem is simplified considerably if it is assumed that the distortion from O_h symmetry is sufficiently strong that the splitting of the $^4T_{1g}$ term leaves a well isolated orbital singlet as the ground state [13]. Under this assumption the magnetic properties may be analyzed according to the Wagner–Friedberg model with $S = 3/2$ [8] or the Weng model with the coefficients generated by Hiller *et al.* [10] for $S = 3/2$. The best fit parameters utilizing these models are given in Table 7. In this case the Wagner–Friedberg model not only reproduces the position of the susceptibility maximum better than the other model it also produces a slightly better fit overall. The best-fit curve calculated using the Wagner–Friedberg model is shown in Fig. 4. Clearly there is a discrepancy between the general shapes of the experimental and calculated curves; moreover the deviation of the g value (2.43) from the spin-only value (2.002) shows that the orbital contribution to the susceptibility cannot be totally 'quenched' as is assumed by the model.

TABLE 7. Magnetic parameters for $Co(HCONH_2)_2[H(C_6H_5)PO_2]_2$

Model[a]	S	g	$-J$ (cm^{-1})	F [b]
W	3/2	2.41	1.35	0.0580
W–F	3/2	2.43	1.58	0.0522
W	1/2	5.30	5.16	0.0635
W–F	1/2	5.43	7.90	0.0522
I	1/2	5.11	6.95	0.0812
W[c]	1/2	4.87	4.39	0.0249
W–F[c]	1/2	5.18	7.17	0.0508
I[c]	1/2	4.60	5.71	0.0297

[a]W = Weng (refs. 9 and 10); W–F = Wagner–Friedberg (ref. 8). [b]F = fitting function defined in ref. 5. [c]Data fitted over range 2–30 K only.

An alternative approach to the interpretation of the magnetic data for six-coordinate cobalt(II), particularly at low temperatures, is to consider that spin–orbit coupling splits the $^4T_{1g}$ term in such a way that the lowest level, a Kramers doublet, is the only thermally occupied level [13, 14]. Under this assumption one needs to consider an effective spin, $S' = 1/2$. The best-fit parameters using the Wagner–Friedberg and Weng models for $S = 1/2$ are given in Table 7. As indicated by the F values the fits are no better than for the $S = 3/2$ models. Both the Weng and the Wagner–Friedberg models employ the isotropic Heisenberg Hamiltonian. We have also analyzed the magnetic data employing the anisotropic Ising model of Fisher [15] for $S = 1/2$ (best-fit parameters given in Table 7); this gives even poorer agreement with experiment.

In treating this cobalt system as an effective spin $S' = 1/2$, thermal population of excited states above the ground Kramers doubled is ignored; hence, the models would be expected to work best at the lowest temperatures. We therefore examined fits to the low temperature data only (2–30 K) utilizing all three $S = 1/2$ models. The fits over this limited temperature range are better for all three with the best fit obtained for the Weng model (Table 7). In addition, the g values obtained in the fits to the low temperature data are lower than those obtained in the fits to all the data and, particularly for the Ising model, approach the expected value of ~4.3 [13, 14]. As the temperature increases above 30 K the experimental susceptibilities become increasingly greater than the calculated ones in all cases; comparison of experiment with theory for the Weng $S = 1/2$ model is illustrated in Fig. 4.

In view of the complexities involved in analyzing this cobalt system no attempt will be made here to speculate on the magnitude of the exchange coupling constants. In order to see if the magnetic behaviour of **1** is typical for phosphinate bridged linear chain compounds of cobalt(II), studies on other phosphinate bridged derivatives are in progress.

Supplementary Material

Supplementary crystallographic material is available from author A.B.

Acknowledgement

Authors J.-L.D., L.S.-M.L. and R.C.T. thank the Natural Sciences and Engineering Research Council of Canada for Financial Support.

References

1 P. Betz and A. Bino, *Inorg. Chim. Acta, 147* (1988) 109, and refs. therein.
2 J. S. Haynes, K. W. Oliver and R. C. Thompson, *Can. J. Chem., 63* (1985) 1111.
3 A. Bino and L. Sissman, *Inorg. Chim. Acta, 128* (1987) L21.
4 J.-L. Du, K. W. Oliver and R. C. Thompson, *Inorg. Chim. Acta, 141* (1988) 19.
5 W. V. Cicha, J. S. Haynes, K. W. Oliver, S. J. Rettig, R. C. Thompson and J. Trotter, *Can. J. Chem., 63* (1985) 1055.
6 H. D. Gillman, *Inorg. Chem., 13* (1974) 1921.
7 J. S. Haynes, K. W. Oliver, S. J. Rettig, R. C. Thompson and J. Trotter, *Can. J. Chem., 62* (1984) 891.
8 G. R. Wagner and S. A. Friedberg, *Phys. Lett., 9* (1964) 11.
9 C. H. Weng, *Ph.D. Dissertation,* Carnegie-Mellon University, Pittsburg, PA, 1968.
10 W. Hiller, J. Strähle, A. Datz, M. Hanack, W. E. Hatfield, L. W. terHaar and P. Gütlich, *J. Am. Chem. Soc., 106* (1984) 329.
11 J. L. Du and R. C. Thompson, *Can. J. Chem., 67* (1989) 1239.
12 B. N. Figgis, M. Gerloch, J. Lewis, F. E. Malbs and G. B. Webb, *J. Chem. Soc. A,* (1968) 2086.
13 V. T. Kalinnikov, Yu. V. Rakitin and W. E. Hatfield, *Inorg. Chim. Acta, 31* (1978) 1.
14 R. L. Carlin, *Magnetochemistry,* Springer, Berlin, 1986.
15 M. E. Fisher, *J. Math. Phys., 4* (1963) 124.